Polymer 50 (2009) 1682–1691

Contents lists available at ScienceDirect

Polymer

journal homepage: www.elsevier.com/locate/polymer

Synthesis and characterization of novel citric acid-based polyester elastomers

Ivan Djordjevic, Namita Roy Choudhury*, Naba K. Dutta, Sunil Kumar

Ian Wark Research Institute, University of South Australia, Mawson Lakes Campus, Mawson Lakes, SA 5095, Australia

ARTICLE INFO

Article history:
Received 2 October 2008
Received in revised form
19 January 2009
Accepted 20 January 2009
Available online 24 January 2009

Keywords:
p(OCS) elastomers
Polyesterification
Citric acid

ABSTRACT

In this paper we report successful simple synthesis of unique elastic polyesters by carrying out catalyst-free polyesterification of multifunctional non-toxic monomers: 1,8-octanediol (OD), citric acid (CA) and sebacic acid (SA). The chemical, physical, and surface chemical properties of the resulting copolyester polyoctanediol citrate/sebacate [p(OCS)] have been investigated. This new material was characterized by matrix-assisted laser desorption/ionisation time-of-flight mass spectrometry (MALDI-ToF-MS), nuclear magnetic resonance spectroscopy (NMR), thermal analysis (TA), mechanical tests, photo-acoustic Fourier-transform infrared spectroscopy (PA-FTIR), X-ray photoelectron spectroscopy (XPS) and swelling experiments. We demonstrate that the chemical structure, morphology, physical integrity and surface chemistry of the synthesized co-polymer can be controlled by simply varying the initial acid concentration (CA/SA) in the pre-polymer. This novel p(OCS) polymer exhibits versatility in mechanical properties, hydration and hydrolytic degradation as determined by the chemical structure of the polyester elastomer.

1. Introduction

In recent years, catalyst-free synthesis has emerged as a potential route to synthesize elastic polyesters with appropriate mechanical integrity, suitable surface characteristics and compatibility for fabrication of tissue engineering scaffolds [1]. Various polyester elastomers, synthesized so far from low-cost and non-toxic precursors such as 1,8-octanediol (OD), citric acid (CA), glycerol and sebacic acid (SA), represent a new generation of advanced biocompatible and biodegradable synthetic materials with potential biomedical applications [2,3]. Their synthesis is realized by polycondensation, a well-defined process of melting polyfunctional alcohols and organic acids for creating polymer networks [4]. Trifunctional citric acid can react with alcohols or polyols to form esters without any catalysis. This reaction is reported to occur via reactive anhydride intermediate [5], followed by its reaction with alcohol with a large extent of intramolecular cross-linking. The probability of such networking can be increased by controlling the concentration of the precursors. The resulting chemical structure and processing determine the physical integrity of the synthesized elastic material [5].

In earlier work, several investigators have reported that scaffolds fabricated from elastic polyesters, in particular polyoctanediol citrate (POC) or polyglycerol sebacate (PGS), are compatible for regeneration of different tissues such as blood vessel [6–8], cartilage [9], bone [10], and nerve tissue [11]. POC-based scaffolds synthesized by the polyesterification reaction between OD and CA, and fabricated by solvent-casting/particulate-leaching technique are permissive to *in vitro* chondrocyte proliferation and formation of extra-cellular matrix (ECM) within the scaffold porous structure [9]. *In vivo* immunological response of polyester elastomer, such as PGS, has shown no gross inflammation or fibrosis [11]. According to Yang et al. the POC elastomers show inflammatory response that is similar to that shown by a standard PLGA with minimal fibrous capsule formation [3]. Apart from their easy thermal processabilities [12], the properties of elastomeric citrates could also be tailored by mixing them with natural bone mineral hydroxy apatite (HA) [10] or with PLLA [13] in order to meet specific tissue regeneration requirements.

In view of the potential of citrate elastomers for tissue engineering applications, here we report the synthesis and characterization of a new class of these materials, polyoctanediol citrate/sebacate [p(OCS)] by a catalyst-free polyesterification of multifunctional OD, CA and SA monomers. We have carefully chosen CA and SA as they are part of natural metabolic cycles in humans and therefore considered to be biocompatible [2,3]. The OD has been

* Corresponding author. Tel.: +61 8 83023719; fax: +61 8 83023683.
E-mail address: namita.choudhury@unisa.edu.au (N.R. Choudhury).

0032-3861/$ – see front matter © 2009 Elsevier Ltd. All rights reserved.
doi:10.1016/j.polymer.2009.01.045

chosen as the difunctional monomer because it is the largest aliphatic diol that is water soluble with no reported toxicity (a feature beneficial to the degradation process) [6,14]. The design and control over the chemical composition of p(OCS) is based on the hypotheses: (i) the variation in the initial CA/SA monomer concentration would yield copolyesters with varying number of CA segments present in the final polymer chains; and (ii) the ratio OD:(SA + CA) when kept 1:1 would lead to a complete polyesterification reaction, where all the OD monomer has reacted with both the SA and CA monomers. The tuning of the final composition has the potential to provide a simple but elegant method to control the final properties of this material [2,15].

2. Experimental

2.1. Synthesis of p(OCS) elastomers and sample preparation

High purity citric acid (CA; molecular weight (M_w) = 192.13 g mol^{-1}; melting temperature (T_m) = 153 °C), sebacic acid (SA; M_w = 202.24 g mol^{-1}; T_m = 134 °C), 1,8-octanediol (OD; M_w = 146.23 g mol^{-1}; T_m = 58–61 °C), dioxane, ethanol (EtOH), sodium iodide (NaI), 2,5-dihydroxybenzoic acid (DHB), deuterated dimethyl sulfoxide (DMSO-d_6) and phosphate buffer pellets were purchased from Sigma–Aldrich and used as received. Poly-octanediol citrate/sebacate p(OCS) polymers were synthesized using the following procedure.

Equimolar amounts of both the OD and acids [OD:(CA + SA) = 1:1] were mixed together to form the pre-polymer mixtures that were then used for further polyesterification reaction. Three different compositions of the monomers were undertaken to produce pre-polymers as depicted in Table 1. The pre-mixed reactants (OD, CA and SA) were placed in a three-necked round-bottom flask and the monomer mixture was first heated up to 160–165 °C followed by mixing at 140–145 °C for 1 h under a constant stream of nitrogen.

The pre-polymers thus obtained were dissolved in dioxane [20% (w/w) solution] and the resulting pre-polymer solutions of all the p(OCS) compositions (Table 1) were used for both scaffold and film preparation without further purification [16]. Scaffold was prepared by particulate-leaching method. Yang et al. used similar approach for the production of porous scaffolds of similar elastomeric polyester material [3]. Films for structural analyses were cast into Teflon™ petri dishes and left in an oven at 80 °C for 7 days for solvent evaporation and further polyesterification of the pre-polymers. The final product, p(OCS) polyester, was prepared in the form of a thin sheet of ~1 mm thickness (thin sheet chosen due to the complexity of characterization of 3D scaffold by many techniques). This sheet was then compression-molded to obtain a sub-millimetre thickness film in a window mold maintained at 150 °C and 15 MPa. While both the pre-polymers and the films were subsequently analysed for their structural properties, no attempt was made to investigate the effect of possible compression-induced physico-chemical changes. Synthesized and processed p(OCS) polyesters exhibit thermoplastic behaviour as confirmed by the repeated moldability. All the films were produced under same reaction conditions and the samples were stored in a desiccator for subsequent tests.

Table 1
Initial molar ratio of the monomers in polyesterification reaction and the p(OCS) pre-polymer mixture composition calculated from deconvolution of ^{1}H NMR spectra.

Monomer ratio (OD:CA:SA)	Nomenclature	NMR peaks (%)			
		H_j^1	H_j^2	H_k^1	H_k^2
1:1:0	$p(O_1C_1S_0)$	28.5	71.5	0	0
1:0.75:0.25	$p(O_1C_{0.75}S_{0.25})$	28.1	71.9	69.4	30.6
1:0.5:0.5	$p(O_1C_{0.5}S_{0.5})$	28.4	71.6	73.1	26.9

2.2. Nuclear magnetic resonance (NMR) spectroscopic analysis

The p(OCS) pre-polymers for NMR analysis were purified by precipitation in water followed by constant mixing, filtering and freeze-drying. The reaction yield was calculated by comparing masses of both non-purified and purified pre-polymers and it was found to be ~80% for all three compositions. The yield appears to be low due to some material loss during filtering process. Small portions of purified pre-polymer mixtures were sampled and dissolved in DMSO-d_6. The ^{1}H NMR spectra were recorded using a Bruker NMR spectrometer (350 MHz). The pre-polymers of three different compositions (Table 1) were dissolved in DMSO-d_6 and the solutions were placed in NMR tubes with 5 mm outer diameter. The chemical shifts were measured relative to the solvent peak as secondary standard.

2.3. Matrix-assisted laser desorption/ionisation (MALDI) time-of-flight mass spectrometry (ToF-MS) analysis

Purified p(OCS) pre-polymers were prepared for MALDI-ToF-MS analysis by dissolving 10 mg of p(OCS) pre-polymers in 1 ml of EtOH. Matrix (DHB) was prepared by dissolving 20 mg in 10 ml of EtOH and the ionising agent NaI (100 mg in 10 ml of EtOH) was used. After optimisation and careful choice of appropriate sample preparation technique, pre-polymers were deposited on MALDI plate by using the layer-by-layer method developed by Meier and Schubert [17]. In brief, the 1.5 μl of EtOH solution of matrix was first deposited and dried on the sample plate. A subsequent layer of prepared NaI solution (1.5 μl) was added on the top of dried matrix. After second drying, the 1.5 μl of polymer solutions was added on the top of the crystallised DHB–NaI mixture. Samples were dried again and placed in MALDI-ToF-MS (Micromass M@LDI LR Instrument from Waters, UK) equipped with a pulsed (4 ns) nitrogen laser emitting at 337 nm. The detector was operated in positive ion mode. The pulse voltage was set to 750 V. At least 20 spectra were collected and combined.

2.4. Scanning electron microscopy (SEM) of citrate scaffold and film

The porous structure and surface morphology of p(OCS) scaffolds and films was analysed using scanning electron microscopy (SEM). The instrument used for analysis was a CamScan SEM (Model CS44FE) equipped with a field emission gun, which was operated at an accelerating voltage of 15 kV. The samples were mounted on a stub with double-sided conductive tape and coated with carbon to avoid surface charging, which affects the secondary electron imaging. The images were recorded in secondary electron mode.

2.5. Thermal analyses of p(OCS) films: thermogravimetric analysis (TGA) and differential scanning calorimetry (DSC)

The thermal properties of p(OCS) elastomers were characterized using TA Instruments (Delaware, USA) TGA (model 2950) and DSC (model 2920). TGA thermograms were obtained under the flow of nitrogen (70 ml min^{-1}) at a scanning rate of 10 °C min^{-1} in the range of 25–500 °C. The onset of degradation temperature (T_{OD}) was determined from the TGA curve at 5% weight loss.

Glass-transition temperature (T_g), crystallisation temperature (T_c) and melting temperature (T_m) of the p(OCS) films were evaluated using DSC at a heating/cooling rate of 10 °C min^{-1}. The sample

film (~10 mg) placed on the aluminium pan was first heated from 40 °C to 150 °C and then cooled from 150 °C to −80 °C, followed by a second heating cycle from −80 °C to 150 °C. All the data from the second heating cycle were used for the analysis of T_g, T_c and T_m. The p(OCS) polymers were also analysed with DSC in their hydrated state. Sample films were soaked in water until they reached equilibrium percentage swelling (as described in Section 2.9) prior to the DSC experiment. Glass transition was evaluated on a small piece of hydrated sample (carefully wiped with Kimwipe™ to remove surface water) by heating in one cycle (−50 °C to 170 °C; heating rate of 10 °C min^{-1}). The reason for higher temperature in this experiment is for an observation of presence of any unreacted monomers within polymer network after curing process.

2.6. Tensile tests

Physical properties of the p(OCS) films were measured using a Hounsfield tensiometer (model: K10KS-0128) equipped with 100 N load cell at room temperature. Briefly, the film samples prepared according to the ASTM standard D 882-01 (45 × 5 × 0.2 mm, length × width × thickness) were tested at a rate of 10 mm min^{-1}. Young's modulus was calculated from the linear part of the initial slope. For each composition (Table 1), the test was performed 5 times. The result was averaged and a standard deviation is reported. The cross-linking density (n) was calculated according to the rubber elasticity theory using the expression: $n = E_0/3RT = \rho/M_c$; where n represents the number of active network chain segments per unit volume (mol m^{-3}), M_c represents the molecular weight between cross-links (g mol^{-1}), E_0 represents Young's modulus (MPa), R is the universal gas constant (8.314 J mol^{-1} K^{-1}), T is the absolute temperature ($T = 298$ K) and ρ is the density. Stress relaxation experiment on the samples was also performed on the same instrument to examine the relaxation characteristics. The experimental procedure involved application of constant strain (60%) followed by relaxation period. All the samples were tested in triplicate at room temperature.

2.7. Photo-acoustic Fourier-transform infrared spectroscopy (PA-FTIR) analysis

The p(OCS) films were analysed by a Nicolet Magna™ IR spectrometer (model 750) equipped with an MTEC (model 300) PA cell. The spectra were collected in the mid-infrared region with 100 scans at a resolution of 8 cm^{-1} and a mirror velocity of 0.158 cm s^{-1}. Carbon black was used as a reference and the system was purged with helium gas at a flow rate of 10 cm^3 s^{-1}.

2.8. X-ray photoelectron spectroscopy (XPS) analysis

The XPS spectra of the p($O_1C_1S_0$) films were recorded using a Kratos AXIS Ultra DLD spectrometer equipped with a monochromatic Al Kα radiation source ($h\nu = 1486.7$ eV) operating at 13 kV and 10 mA. The elements present in the sample surface were identified from a survey spectrum recorded over the energy range 0–1100 eV with a pass energy of 160 eV and a resolution of 0.5 eV. High-resolution (0.1 eV) spectra were then recorded for pertinent photoelectron peaks at a pass energy of 20 eV to identify the chemical state of each element. All the binding energies (BE) were referenced to the C 1s neutral carbon peak at 285 eV, to compensate for the effect of surface charging. The analysis area was 700 × 300 μm. The processing and curve-fitting of the high-resolution spectra were performed using the CasaXPS™ software.

2.9. Swelling experiment

The percentage swelling of the p(OCS) polyester in Milli-Q water and in dioxane was measured as follows: 10 mm diameter discs of the p(OCS) films were punched out from the film and soaked into 15 cm^3 of liquid at room temperature. The discs were taken out of the water and the solvent at various time intervals and their weights measured after wipe-cleaning their surfaces with a lint-free paper. The percentage swelling of the discs was calculated using the expression $[(M_w - M_0)/M_0] \times 100\%$, where M_0 and M_w represent the disc masses in dry and wet conditions, respectively. Each measurement was performed in triplicate and appropriate standard deviations calculated. After the swelling experiments, the discs were dried to constant weight and sol content was calculated using the expression $[(M_0 - M_d)/M_d] \times 100\%$, where M_0 and M_d represent the disc masses in pre- and post-swelling (dried) states.

2.10. Hydrolytic degradation

The hydrolytic degradation examined by measuring the percentage degradation in phosphate buffer solution (PBS) at 37 °C was evaluated by the following procedure: The 10 mm diameter discs, punched from the p(OCS) films, were soaked in 10 ml of PBS and kept in a water bath at constant temperature. Samples were taken out on one week intervals and dried to their constant weight. The PBS was replaced upon sampling each week. The percentage degradation was calculated using the expression: $[(M_0 - M_d)/M_0] \times 100\%$, where M_0 is a sample mass prior to degradation and M_d is a sample mass after drying to a constant weight. Each measurement was performed in triplicate and appropriate standard deviations calculated.

3. Results and discussion

3.1. Chemical structure by NMR spectroscopic analysis

Fig. 1 shows the ^{1}H NMR spectra of representative purified p(OCS) pre-polymers with varying initial molar ratios of CA/SA. A proposed structural formula for the resulting copolyester in Fig. 1 shows the correlation between the various structural components and the observed NMR peaks. Similar assignment has also been reported by others [3,14,18]. In brief, peak "a" is assigned to esterified –OH group from OD which is shifted towards lower values (triplet at 3.3–3.4 ppm) in comparison to the NMR spectrum of pure OD (triplet peak at 4.3 ppm). In this experiment we could not identify terminal OD segments that are expected to appear towards higher chemical shifts [19]. However, other peaks that correspond to CA (peaks "i" and "j") and SA segments (peak "k") in pre-polymer chains show splitting that is most likely a consequence of existing CA and SA terminal groups [19]. Both peaks are composite of 2 triplets and the deconvolution of those peaks is shown as insets in Fig. 1 (calculated values from peak areas are reported in Table 1). Our NMR results indicate the existence of both terminal and fully esterified acid groups in p(OCS) pre-polymers. The triplets shift towards higher values corresponds to terminal acid (CA and SA) segments and this observation is in line with MALDI-ToF-MS results discussed in the following section.

3.2. Molecular weight and structural composition analysis by MALDI-ToF-MS

The molecular weights (M_w) of p(OCS) pre-polymers were determined by MALDI-ToF-MS analysis and the spectra corresponding to the different CA/SA ratios are shown in Fig. 2. Each spectrum shows unimodal distribution of ions characteristic for

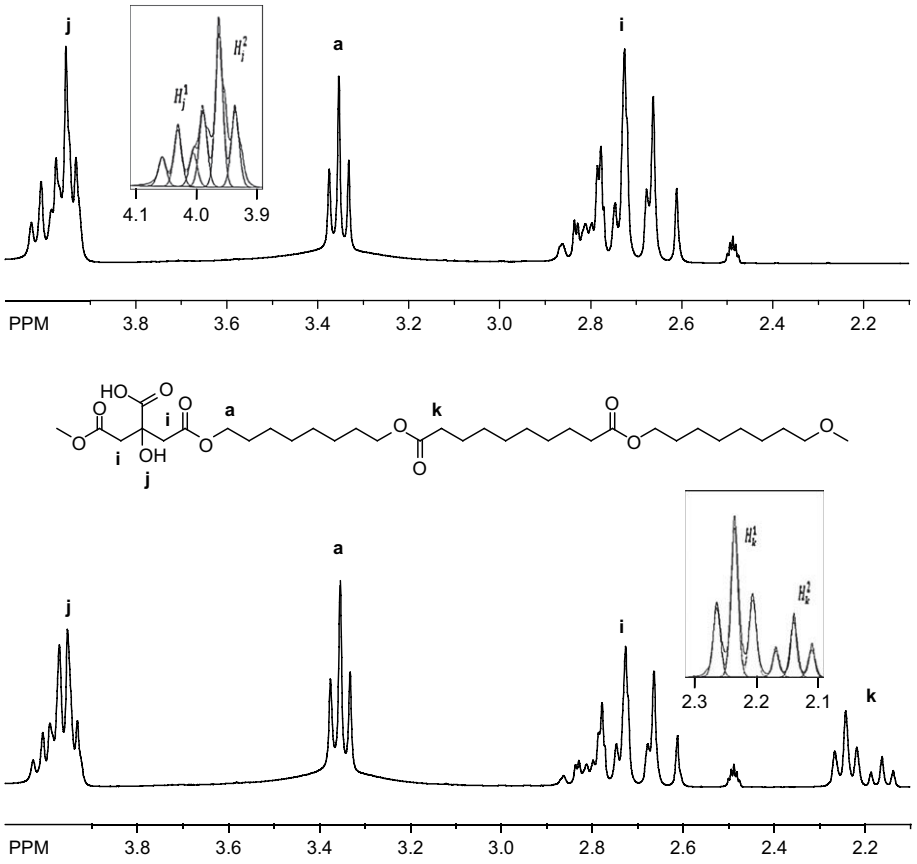

Fig. 1. ^{1}H NMR spectra of p(OCS) pre-polymers: (top) p($O_1C_1S_0$); (bottom) p($O_1C_{0.75}S_{0.25}$).

a step-growth polymerization such as polyesterification reaction [20]. The molecular weights of $[p(OCS)+Na]^+$ ions, in the range between 947 and 1409, were calculated from MALDI spectra and the corresponding theoretical and experimental m/z values are reported in Table 2. In Fig. 2, the p($O_1C_1S_0$) composition is consistent with CA/OD alternating segments with increasing number of monomer units from 6 ($m/z = 947$) to 9 ($m/z = 1379$). The differences between each m/z value of this particular composition are 128 and 174 which are dehydrated monomers OD and CA respectively. Other compositions shown in Fig. 2, that involve SA monomers [p($O_1C_{0.75}S_{0.25}$) and p($O_1C_{0.5}S_{0.5}$)], also form polyester linear chains with alternating SA/OD/CA units (6–9) distributed as random blocks. Our results indicate that the ratio between CA and SA can vary within formed polymer, maintaining the same number of overall OD/CA/SA units in citrate/sebacate pre-polymer. Here, for the first time we report MALDI-ToF-MS analysis for such polymers, which clearly shows exclusion of side chain formation reported by others [18]. Free carboxyl groups from CA segments are also likely to exist on p(OCS) surface after curing of the pre-polymers in both film and scaffold form, which is a feature of significant importance for their future biomaterial application [21].

3.3. Surface morphology of scaffold and films by SEM

Fig. 3(a and b) shows the optical photograph of the representative p(OCS) elastomer scaffold and film obtained after compression molding. The elastic nature of the porous scaffold can be clearly evident from the figure as it bounces back against the notch test (Fig. 3(a)). It must be pointed out that both the film and the scaffold have been produced from the same pre-polymer solution. Fig. 3c and d show the SEM images of the representative p($O_1C_1S_0$) scaffold and film respectively (other polymer compositions can be fabricated in the same fashion). The surface of p(OCS) elastomer (Fig. 3(d)) shows micro-wrinkled pattern characteristic of elastomeric surfaces [22]. The average pore diameter in the scaffold ranges from 200 to 300 μm (Fig. 3(c)) and the pores are homogeneously dispersed in the scaffold [6–8]. This study shows that our synthesis method can be used to produce elastic scaffolds for further tissue engineering applications. Detailed analysis of scaffolds and their compatibility in tissue cultures will be reported in a separate study.

3.4. Thermal transitions and degradation of polymers

Thermal stability of the elastomer films synthesized was characterized using TGA (results available in supporting Section 1). The shape of the TGA curves reveals a two-step degradation process for all the examined samples; and indicates high stability and high degree of polymerization without any low M_w residue. Other important structural feature is that the thermal stability of the p(OCS) increases with increasing the concentration of SA in the polymer.

Thermograms of the p(OCS) films were recorded by DSC (Fig. 4) in order to analyse the influence of the pre-polymer composition (determined by NMR and MALDI-ToF-MS) on the morphology of the final product. Glass-transition temperatures (T_g) are determined for all the samples, which is considered to be an important characteristic and reveals the molecular dynamics of polymer chains within a given temperature range. As shown in Fig. 4, all the synthesized p(OCS) polyesters show T_g below room temperature, a characteristic feature that determines their elastomer-like

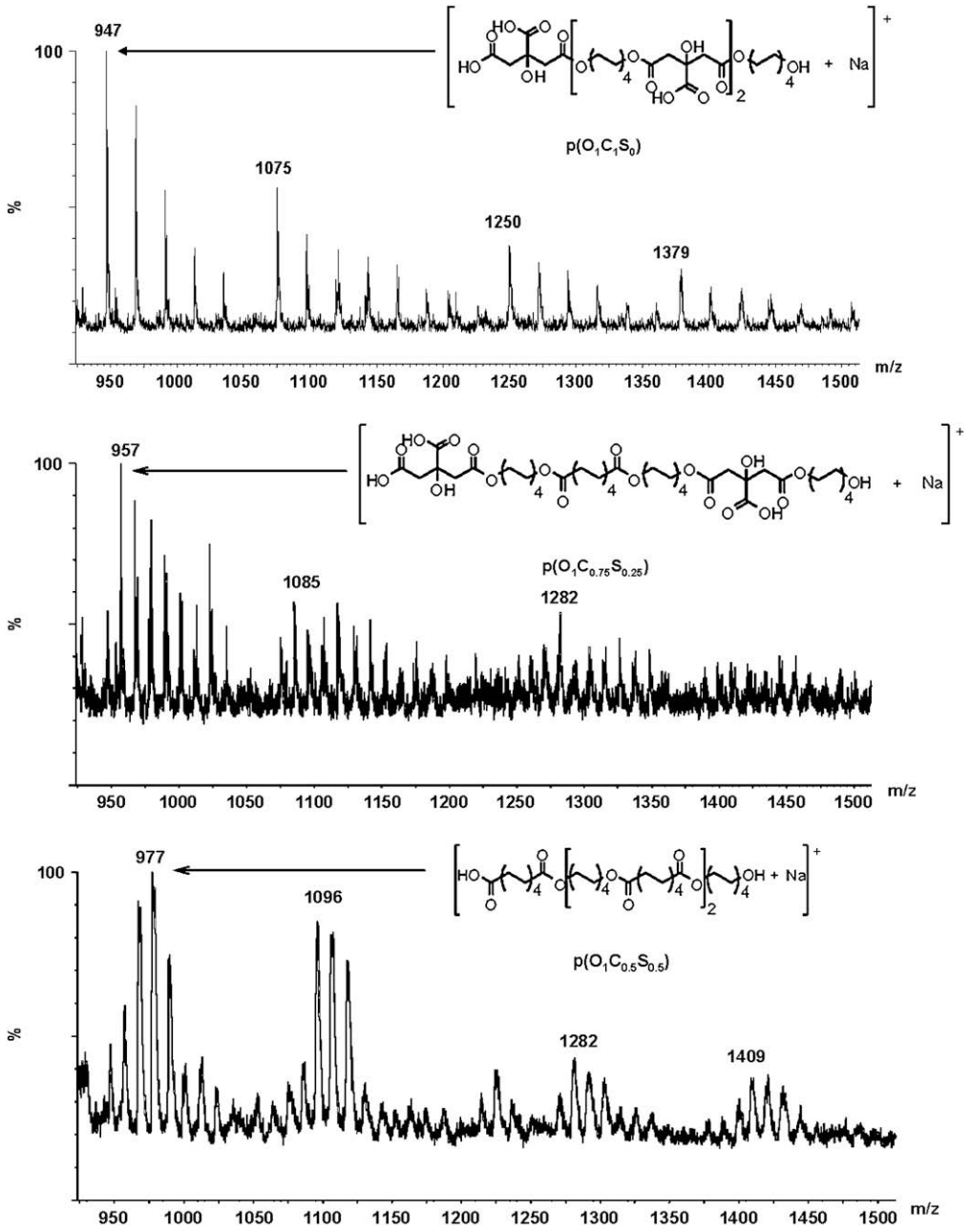

Fig. 2. MALDI-ToF-MS spectra of p(OCS) pre-polymers.

behaviour [16]. Elasticity is caused by high mobility of the macromolecules at temperatures above T_g [23]. In the case of p(OCS), T_g progressively increases with increasing initial concentrations of CA in the reaction mixture. Polymer chains formed from the pre-polymers with higher number of CA segments (Fig. 2) are expected to have strong intermolecular interaction, resulting in reduced molecular segmental dynamics and increasing T_g [3]. Fig. 4 shows a thermogram of the p($O_1C_{0.5}S_{0.5}$) sample that exhibits the lowest T_g value. When temperature is increased above the T_g, molecular motion in this particular sample allows further molecular organization and exhibits a cold crystallisation [24] at $T_c \approx -18\,^{\circ}C$. This particular sample displays a crystalline melting at $T_m \approx 28\,^{\circ}C$, which is also confirmed by visual observation. When held at room temperature within the range of 20–25 °C, the p($O_1C_{0.5}S_{0.5}$) sample appears as a cloudy, non-transparent white film, which retains its elastic integrity similar to the other sample films (Fig. 3). However, on heating over 28 °C, the sample instantly becomes transparent, indicating a transition from partially crystalline to amorphous state. The semi-crystalline morphology of p($O_1C_{0.5}S_{0.5}$) is most likely a result of the formation of longer aliphatic segments generated by polyesterification between OD and SA. In order to confirm that no unreacted monomers are present, we have performed the DSC experiment in one heating cycle (25–170 °C) for all synthesized polymers. No new peaks due to the presence of monomers have been detected.

Thermograms of hydrated p(OCS) samples were also recorded by DSC. All polymer compositions showed consistently lower glass transitions with the decrease in T_g of −40 °C (Fig. 5), −25 °C and −3 °C for p($O_1C_1S_0$), p($O_1C_{0.75}S_{0.25}$) and p($O_1C_{0.5}S_{0.5}$) respectively. Thermogram displayed in Fig. 5 (inset) also shows the melting peak

Table 2
Assignment of molecular weights of Na-cationised p(OCS) pre-polymers detected by MALDI-ToF-MS.

Polymer	Composition	m/z $[M+Na]^+$	
		Experimental	Theoretical
$p(O_1C_1S_0)$	$(CA–OD)_3$[a]	947	947
	$OD–(CA–OD)_3$	1075	1075
	$(CA–OD)_4$	1250	1249
	$OD–(CA–OD)_4$	1379	1377
$p(O_1C_{0.75}S_{0.25})$	CA–OD–SA–OD–CA–OD	957	957
	$OD–SA–OD–(CA–OD)_2$	1085	1085
	$OD–CA–OD–(SA–OD)_2–SA$	1282	1279
$p(O_1C_{0.5}S_{0.5})$	$(SA–OD)_3$	977	977
	$OD–(SA–OD)_2–CA–OD$	1096	1095
	$OD–(SA–OD)_2–CA–OD–SA$	1282	1279
	$OD–(SA–OD)_3–CA–OD$	1409	1407

[a] CA = citric acid segment; OD = 1,8-octanediol segment; SA = sebacic acid segment.

between −10 °C and 0 °C which indicates the presence of water within the $p(O_1C_1S_0)$ polymer network. The shift in glass-transition temperature indicates an increase in molecular motion and therefore, increased elasticity due to a presence of water molecules that act as a plasticizer [25,26]. Such behaviour is well described by Couche-Retszner treatment [27] for polymer–diluent systems which also applies for hydrated elastomeric polymers [28].

3.5. Mechanical properties

Fig. 6(a) shows the tensile stress–strain curves of the p(OCS) films which exhibit typical characteristics of elastic materials [16].

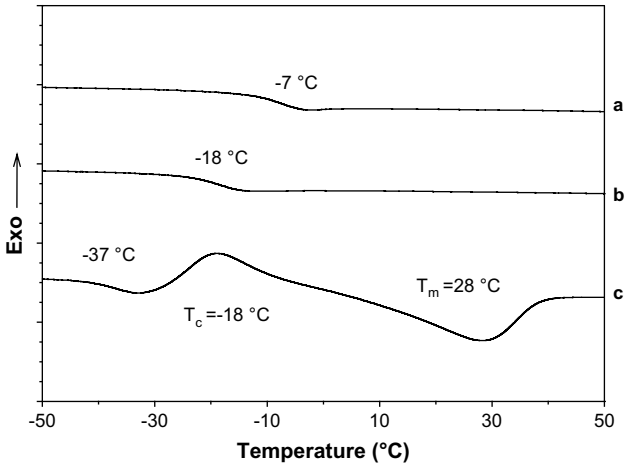

Fig. 4. Glass-transition temperatures (T_g) determined by DSC: a) $p(O_1C_1S_0)$; b) $p(O_1C_{0.75}S_{0.25})$; c) $p(O_1C_{0.5}S_{0.5})$.

The highest value of Young's modulus was recorded for the $p(O_1C_{0.5}S_{0.5})$ sample as displayed in Table 3. This particular structure also exhibits highest elongation during tensile stretching (230%). Due to the semi-crystalline nature of this particular polymer composition, the $p(O_1C_{0.5}S_{0.5})$ represents boundary conditions between elastomeric and crystalline polymers. For that reason, results in Table 3, calculated for $p(O_1C_{0.5}S_{0.5})$, represent an approximation to rubber elasticity theory that is used to describe all three structural compositions. According to the rubber elasticity theory, the $p(O_1C_{0.5}S_{0.5})$ film shows the highest number of active

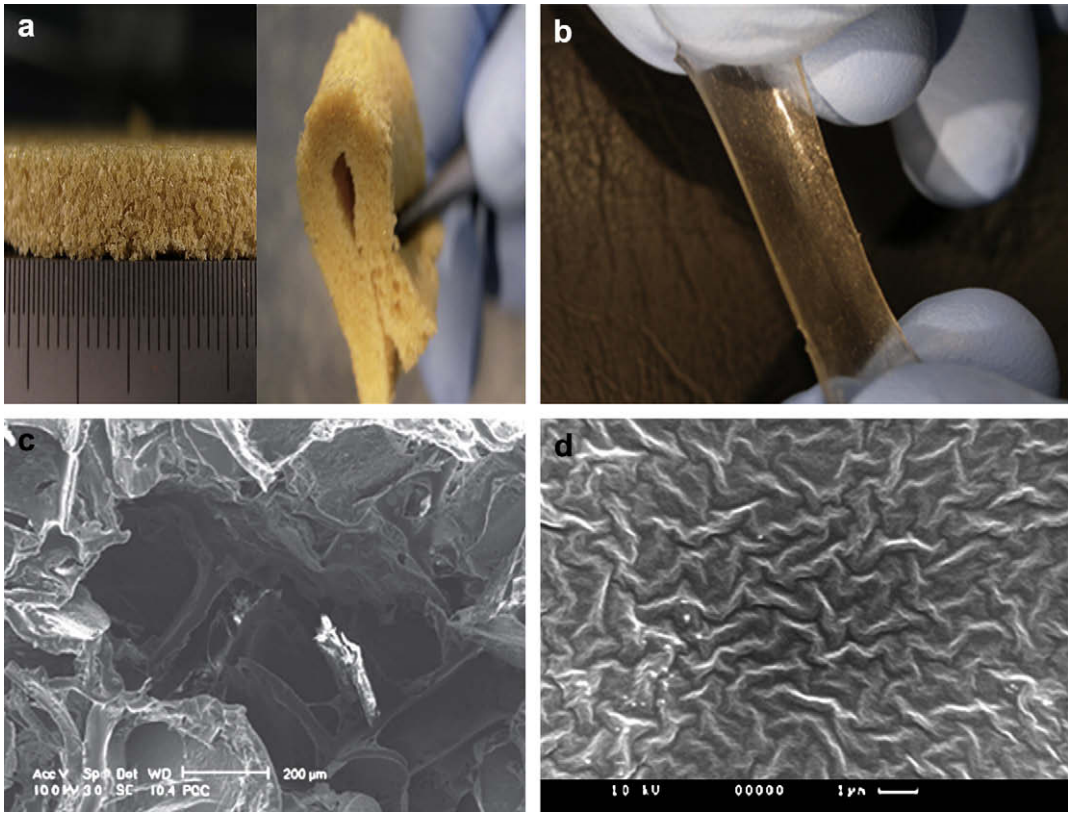

Fig. 3. Photographs and SEM images of representative $p(O_1C_1S_0)$ elastomer: a) porous scaffold produced by particulate-leaching technique (not to scale); b) film obtained by compression molding (not to scale); c) SEM image of the scaffold; d) SEM image of the film (scale bar: 1 µm).

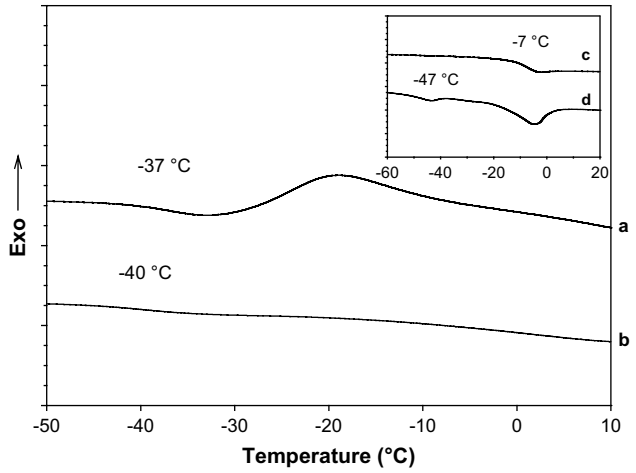

Fig. 5. Thermal behaviour upon hydration measured by DSC for $p(O_1C_{0.5}S_{0.5})$: a) dry; b) hydrated [inset showing a T_g depression upon hydration of $p(O_1C_1S_0)$: c) dry; d) hydrated].

chain segments (n) and therefore the lowest molecular weight between cross-links (M_c). Increase in Young's modulus is characteristic of an increase in intermolecular bonding within the examined material. In case of $p(O_1C_{0.5}S_{0.5})$ polyester, the high level of intermolecular bonding is most likely a result of close packing of molecules within crystalline segments.

These mechanical testing results show that pre-determined chemical structure of the p(OCS) thermoplastic elastomers could be used to tailor their mechanical stiffness for future biomedical applications. Fig. 6(b) shows the time dependent stress relaxation behaviour of all the samples at room temperature. The plot displays general viscoelastic behaviour typical of elastomeric material. Two zones of relaxation are visible in all cases: an initial period, where relaxation is linear and rapid with time followed by a gradual steady zone of equilibrium plateau. Thus, all the samples show a similar shape in stress relaxation pattern. During early stage, rate of relaxation is high as the material continues to recover and reaches a steady state. The percentage relaxation values lie within the range of 10–20% for all samples regardless of their tunable composition. Such behaviour indicates that all studied p(OCS) copolyesters are not only chemically cross-linked elastic material, but also low relaxation is primarily due to greater degree of association and entanglement. Strong level of interaction prevents molecules from sliding over one another effectively. As such primary covalent bonds are difficult to break and are not likely to contribute to the stress relaxation property. This result also demonstrates that these p(OCS) materials possess both chemical and physically cross-linked chains imparting thermoplastic elastomeric characteristics and the relaxation behaviour [28].

3.6. Surface analysis by PA-FTIR

The infrared spectrum of the representative p(OCS) films, obtained using the PA-FTIR instrument, is shown in Fig. 7. The 1735 cm^{-1} peak corresponding to the –C═O vibration of ester bonds confirms the formation of the polyester [3,14,29,30]. Broad bands centred at 3440 cm^{-1} and 3295 cm^{-1} are assigned to hydrogen-bonded hydroxyl groups stretching vibration and the O–H vibration (ν_{O-H}) of the hydrogen-bonded carboxyl groups from CA segment, respectively [3]. Inset spectra in Fig. 7 show increased intensity of the hydroxyl peaks with increase in the number of CA segments in the p(OCS) chains. These results suggest that the density of the hydrogen-bonded hydroxyl groups in the p(OCS) polymers is determined by the CA/SA concentration ratio, which primarily determines the interaction of the p(OCS) with water. This is also supported by our swelling results (Section 3.8). Therefore, the $p(O_1C_1S_0)$ composition with the highest number of CA segments is expected to be most hydrated.

3.7. Surface analysis by XPS

The XPS analysis was performed in order to investigate the presence, in general, of pendant carboxyl groups in the p(OCS) elastomers. Only one of the four types of samples [$p(O_1C_1S_0)$] has been investigated as a representative material for the XPS study. A survey photoelectron spectrum of the $p(O_1C_1S_0)$ sample is displayed in Fig. 8(a), showing the carbon (C 1s) and oxygen (O1s) photoelectron signals with small quantities of impurities (1.4 at. % Si; 0.4 at. % F; 0.3 at. % N and; 0.1 at. % Ag). A high-resolution C 1s spectrum of this sample, when curve fitted, can be seen as consisting of three major components, as shown in Fig. 8(b). The first component at ~285 eV is attributed to the aliphatic carbon (–C–C–) bonds and carbon–hydrogen bonds (–C–H–). Chemical shifts were calculated relative to the aliphatic peak. The C 1s component shifted by 1.7 eV is attributed to the ester bonds (–C–O–C═O) and the component shifted by 4.3 eV is assigned to the carboxyl groups (–COOH) [31]. It is estimated from the various peak areas of the C 1s curve-fitted spectrum [Fig. 8(b)] that the chemical functionalities at the surface of the $p(O_1C_1S_0)$ sample are

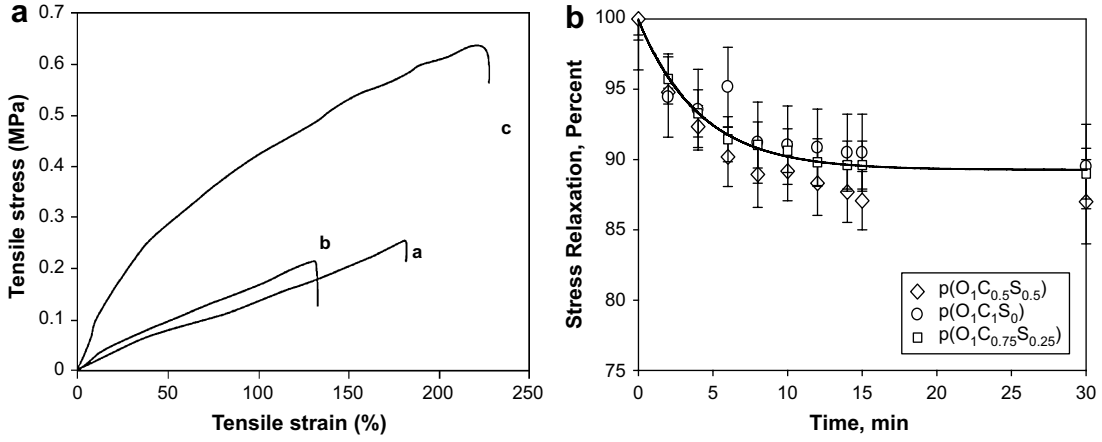

Fig. 6. (a) Stress–strain curves for p(OCS) films: (a) $p(O_1C_1S_0)$; (b) $p(O_1C_{0.75}S_{0.25})$; (c) $p(O_1C_{0.5}S_{0.5})$; (b) Stress relaxation characteristics of the P(OCS) copolyesters.

Table 3
Physical and mechanical properties of p(OCS) polymer films.[a]

Polymer	Density (g cm^{-3})	Young's modulus (MPa)	Elongation (%)	Tensile strength (MPa)	n (mol m^{-3})	M_c (g mol^{-1})
$p(O_1C_1S_0)$	1.09 {0.01}	0.19 {0.01}	168 {11}	0.24 {0.02}	26 {1}	41,923 {1999}
$p(O_1C_{0.75}S_{0.25})$	1.11 {0.02}	0.20 {0.02}	127 {15}	0.20 {0.02}	27 {4}	41,111 {4239}
$p(O_1C_{0.5}S_{0.5})$	1.12 {0.02}	1.10 {0.30}	231 {11}	0.63 {0.09}	148 {36}	7568 {1976}

[a] Mean values are reported with the standard deviation in brackets.

mainly composed of aliphatic segments (~65%), with polyester and carboxyl groups contributing ~21% and ~13%, respectively. This estimation is in good agreement with the other structural investigations we have carried out. Presence of carboxyl groups is likely to originate from CA, which has two primary and one tertiary carboxyl acid groups, which is less reactive than primary acid groups [5]. In addition, it has also a tertiary hydroxyl group in sterically hindered position. A combination of all these free functional groups eventually influences the hydrogen bond interactions, swelling and hydration of p(OCS) elastomers.

3.8. Swelling characteristics

The swelling behaviour of the p(OCS) samples in water is shown in Fig. 9. Samples soaked in water reach their swelling equilibrium within hours with maximum swelling degree up to 14% for $p(O_1C_1S_0)$. Sol content has been calculated to be 2–5% for all the samples (data not shown). Since no unreacted monomers have been detected in thermal analysis, the sol content evaluated in this experiment can only be attributed to the possible formation of short oligomers soluble in water. Although no such formation could be detected in our DSC analysis, the relatively small amount of the sol content, detected in swelling experiment, provides a clear indication of successful polymer network formation from the pre-polymer mixtures.

Our swelling experiments illustrate how equilibrium percentage swelling drops with decreasing concentration of CA (Fig. 9). This particular result suggests that in the case of p(OCS) polyester elastomers, hydration is dependent on the number of hydrophilic functionalities such as carboxyl and hydroxyl groups (as we have determined from PA-FTIR, and XPS) present. The swelling experiment also reveals that the samples with longer hydrophobic aliphatic chains have less percentage swelling in water. The sample with composition $p(O_1C_{0.5}S_{0.5})$ shows lowest hydration due to the strong presence of aliphatic hydrophobic segments generated from polyesterification between OD and SA. This finding is consistent with the results reported in the DSC experiment. Polyester with structure $p(O_1C_{0.5}S_{0.5})$ exhibits semi-crystalline behaviour, which does not allow water to penetrate causing low percentage swelling (Fig. 9). Although our results show disappearance of crystallisation upon swelling (Fig. 5), the $p(O_1C_{0.5}S_{0.5})$ composition is consistent of longer aliphatic chains and is expected to express lowest hydrophilicity. In the present case, replacing CA with SA as a building block in copolyester formation leads to increased swelling in water, that is, by simply varying the CA/SA ratio in the pre-polymer composition (Table 1). With our synthesis method and material processing technique, we are able to successfully control both

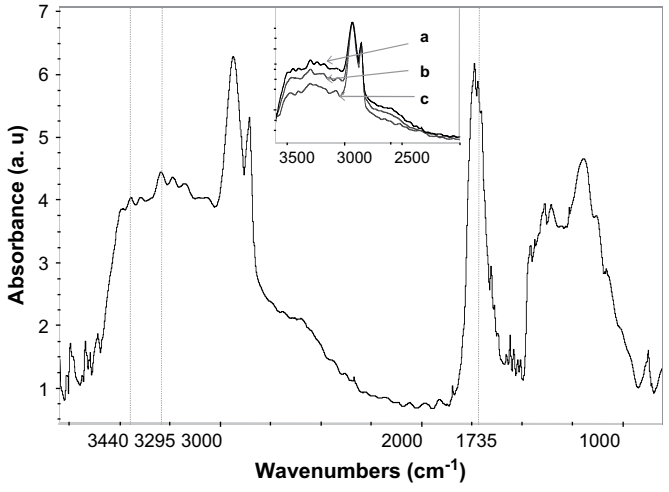

Fig. 7. Representative PA-FTIR spectrum of p(OCS) elastomer [inset showing an increase of 3440 cm^{-1} and 3295 cm^{-1} peaks corresponding to hydrogen-bonded –OH functionalities: (a) $p(O_1C_1S_0)$; (b) $p(O_1C_{0.75}S_{0.25})$; (c) $p(O_1C_{0.5}S_{0.5})$].

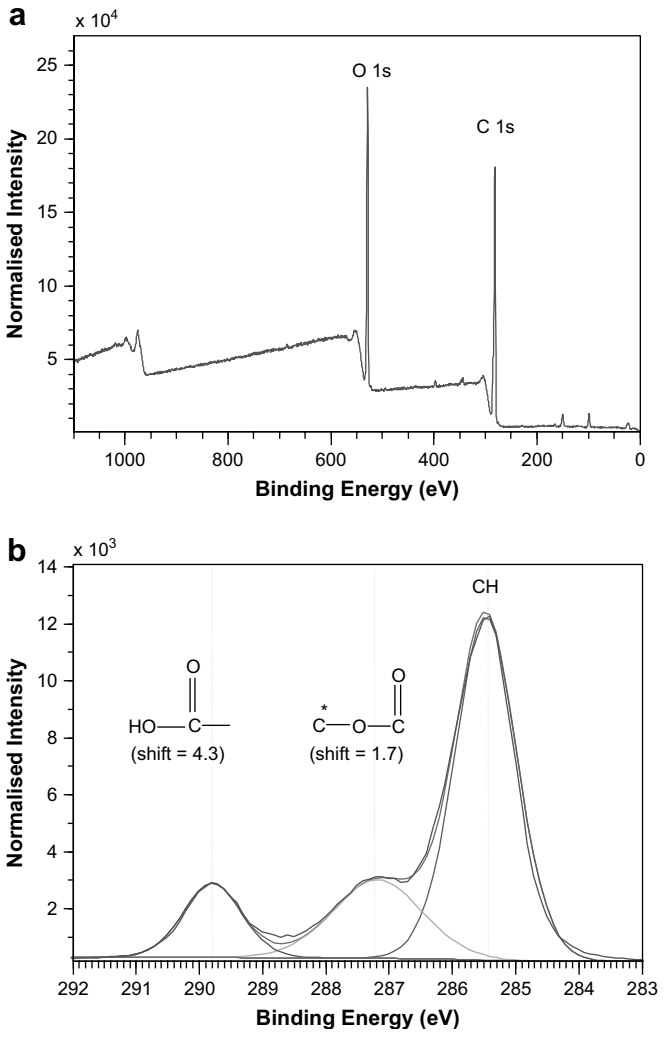

Fig. 8. XPS spectra of a $p(O_1C_1S_0)$ film sample: (a) survey spectrum; (b) high-resolution C 1s region.

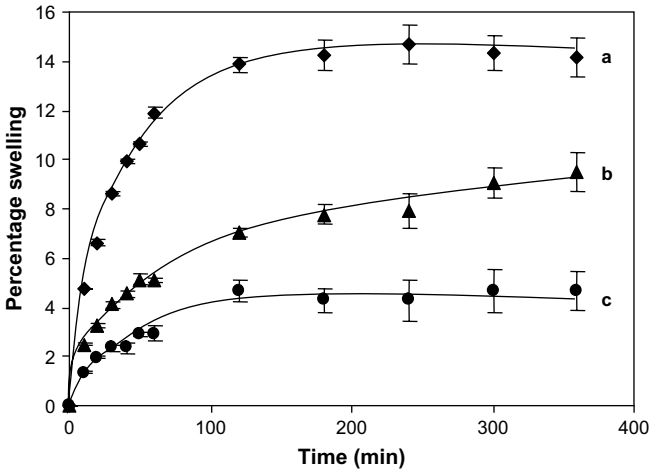

Fig. 9. Percentage swelling of the p(OCS) elastomer films in water: a) $p(O_1C_1S_0)$; b) $p(O_1C_{0.75}S_{0.25})$; c) $p(O_1C_{0.5}S_{0.5})$.

mechanical properties, processability and hydration of the p(OCS) elastomers. In general, the material can be made elastic through covalent cross-links, 3D networks of random coil via the hydroxyl and carboxyl groups attached to the backbone (Fig. 2). Extensive hydrogen bonding between adjacent chain hydroxyl and carboxyl groups also plays a crucial role to attribute unique elastomeric properties. By cumulative hydrogen bond interactions, it is possible to create strongly bound supramolecular polymer and three dimensional structures. In such system, the monomeric units are held together by non-covalent interactions (labile crosslink), thus providing unique opportunities for designing tunable materials [32]. Thus extensive hydrogen bonding prevalent in these copolyesters makes them versatile for use in biomedical field. It is noteworthy that the hydration is an important feature for interaction of biomaterials with biological systems. Another important feature of this material is that the samples retain their physical integrity upon swelling in water.

In order to confirm the nature of interaction in the final polymers, equilibrium swelling experiment was performed using dioxane (same solvent used for making pre-polymer solutions). A disk was made from each sample, and kept in the solvent at room temperature for 7 days. It is interesting to note that all 3 p(OCS) compositions show equilibrium swelling in the range of 250–290% with sol content of 5–7% (data not shown). Such a high percentage swelling not only indicates the close matching of the solubility parameter of the solvent ($20.2\ J^{1/2}\,cm^{-3/2}$) and the polymer ($21.5\ J^{1/2}\,cm^{-3/2}$) [33] but also the fact that there is a degree of intermolecular interaction in these polymers in addition to chemical cross-links. Although dioxane does dissolve shorter copolyester p(OCS) chains (pre-polymers), the final (post-polymerised) p(OCS) samples do not dissolve in dioxane even after soaking for several days. Relatively small sol content indicates that there is very little presence of small oligomers trapped within p(OCS) network. As the polymer–polymer intermolecular forces are high due to cross-linking and strong hydrogen bonding, the samples do not completely dissolve. However, if these forces are overcome by the introduction of strong polymer–solvent interactions, then dissolution can take place. The process of swelling thus results from the balance of repulsive and attractive forces, which also takes into account the thermodynamic mixing between the net polymer and the solvent; the hydrogen bond interaction between functional groups and the elastic force of the polymer and also inter-chain attractive forces. The expansion of the polymer takes place due to the entropic diffusion of its constituent chains and the solvent. On the other hand, swelling is counterbalanced by elastic forces within the polymer chain and inter-chain attractive forces. As a result, polymer–solvent systems tend to reach the minimum of the Gibbs energy of mixing, which is the driving force of the process. Hence, high percentage swelling in dioxane reveals weakening of intermolecular interactions and physical cross-links between the polymer chains that are disrupted during swelling process. The solvent is able to disrupt extensive hydrogen bonds that are formed between residual functional groups (–OH and –COOH) as well as hydrophobic interactions between aliphatic OD–SA segments thus causing swelling almost 3 times of the original sample mass. This result is consistent with the findings of surface analysis performed by PA-FTIR and XPS, which reveal presence of residual free –OH and –COOH functionalities. It is widely known that non-covalent physical cross-links can be disrupted either by solvent interaction or by heating. The formation of physical cross-links is characteristic of thermoplastic elastomers in general [23]. This class of polymers can be defined as materials that have the performance of the cross-linked elastomers at room temperature and processability of the thermoplastic materials at elevated temperature [28]. In case of our p(OCS) thermoplastic elastomer, all three chemical compositions show consistent swelling behaviour in dioxane and thermal processability as the synthesized p(OCS) films can be recycled and thermally remolded a number of times. Similar type of polyester bioelastomer with thermal processing ability has been reported by Liu et al. [12].

3.9. Hydrolytic degradation

All p(OCS) polymers were degraded in PBS solution at 37 °C. Samples exhibit dry weight loss of $70.1 \pm 8.3\%$, $64.1 \pm 5.8\%$ and $8.6 \pm 1.6\%$ for $p(O_1C_1S_0)$, $p(O_1C_{0.75}S_{0.5})$ and $p(O_1C_{0.5}S_{0.5})$ respectively (degradation profile available in supporting Section 2). This result corresponds to the swelling data recorded for p(OCS) polymers. As expected, the $p(O_1C_{0.5}S_{0.5})$ displays the slowest degradation rate due to the existence of longer hydrophobic chains that do not allow molecules of water to penetrate into the structure thus causing the cleavage of ester bonds. However, the detailed study such as one performed by Tatai et al. is necessary in order to optimise the polymer for future biomedical applications [34]. Similar to the p(OCS) material studied here, PGS and POC elastomers have been studied by other investigators for their potential use in tissue engineering applications [2,11,13,15,35]. Synthesis of all these materials is via catalyst-free polyesterification, and their structural properties are also similar and potentially suitable for fabrication of tissue engineering scaffolds. Wang et al. [35] have monitored *in vivo* degradation of PGS and results show that the degradation is caused by surface erosion. Since our p(OCS) elastomers have structural properties and equilibrium percentage swelling comparable to PGS elastomers [2], we expect that the p(OCS) elastomers would degrade *in vivo* in a fashion similar to that observed for PGS [35]. The key advantage of our p(OCS) elastomer over PGS is its tuneable elastic properties, mechanical strength and hydration characteristics.

4. Conclusion

A new type of copolyesters has been synthesized by a simple catalyst-free polyesterification process with 1,8-octanediol (OD), citric acid (CA) and sebacic acid (SA) as starting monomers. The developed material is elastomeric in nature, which is evident from thermal and mechanical analysis. The thermoplastic behaviour and thermal stability enable the p(OCS) polyesters to be prepared at any required geometry. The chemical, physical, and physico-chemical characteristics such as chemical structure, strength and elasticity,

morphology, and hydration of p(OCS) elastomers can be easily and precisely controlled to suit applications in tissue engineering and drug delivery. The presence of carboxyl and hydroxyl groups at the elastomeric surface can be exploited further for imparting bio-functionality to the polymer, for example attaching biomolecules such as proteins. We believe that this new material will significantly improve the ease of fabrication and performance of biocompatible elastomers for future tissue engineering applications.

Acknowledgement

The authors wish to acknowledge the funding from Australian Research Council, ARC for part support of this work.

References

[1] Webb AR, Yang J, Ameer GA. Expert Opinion on Biological Therapy 2004;4(6):801–12.
[2] Wang Y, Ameer GA, Sheppard BJ, Langer R. Nature Biotechnology 2002;20(6):602–6.
[3] Yang J, Webb AR, Pickerill SJ, Hageman G, Ameer GA. Biomaterials 2006;27(9):1889–98.
[4] Nagata M, Tanabe T, Sakai W, Tsutsumi N. Polymer 2008;49(6):1506–11.
[5] Noordover BAJ, Duchateau R, van Benthem RATM, Ming W, Koning CE. Biomacromolecules 2007;8(12):3860–70.
[6] Yang J, Webb AR, Ameer GA. Advanced Materials 2004;16(6):511–6.
[7] Gao J, Crapo PM, Wang Y. Tissue Engineering 2006;12(4):917–25.
[8] Yang J, Motlagh D, Webb Antonio R, Ameer Guillermo A. Tissue Engineering 2005;11(11–12):1876–86.
[9] Kang Y, Yang J, Khan S, Anissian L, Ameer GA. Journal of Biomedical Materials Research, Part A 2006;77A(2):331–9.
[10] Qiu H, Yang J, Kodali P, Koh J, Ameer GA. Biomaterials 2006;27(34):5845–54.
[11] Sundback CA, Shyu JY, Wang Y, Faquin WC, Langer RS, Vacanti JP, et al. Biomaterials 2005;26(27):5454–64.
[12] Liu Q, Tian M, Ding T, Shi R, Zhang L. Journal of Applied Polymer Science 2005;98(5):2033–41.
[13] Webb AR, Kumar VA, Ameer GA. Journal of Materials Chemistry 2007;17(9):900–6.
[14] Lei L, Ding T, Shi R, Liu Q, Zhang L, Chen D, et al. Polymer Degradation and Stability 2007;92(3):389–96.
[15] Bettinger CJ, Orrick B, Misra A, Langer R, Borenstein JT. Biomaterials 2006;27(12):2558–65.
[16] Nijst CLE, Bruggeman JP, Karp JM, Ferreira L, Zumbuehl A, Bettinger CJ, et al. Biomacromolecules 2007;8(10):3067–73.
[17] Meier MAR, Schubert US. Rapid Communications in Mass Spectrometry 2003;17(7):713–6.
[18] Barroso-Bujans F, Martinez R, Ortiz P. Journal of Applied Polymer Science 2003;88(2):302–6.
[19] Chikh L, Tessier M, Fradet A. Polymer 2007;48(7):1884–92.
[20] Adamus G, Rizzarelli P, Montaudo MS, Kowalczuk M, Montaudo G. Rapid Communications in Mass Spectrometry 2006;20(5):804–14.
[21] Li B, Ma Y, Wang S, Moran PM. Biomaterials 2005;26(24):4956–63.
[22] Ohzono T, Matsushita SI, Shimomura M. Soft Matter 2005;1(3):227–30.
[23] Sperling LH. Introduction to physical polymer science. 3rd ed. John Wiley & Sons, Inc.; 2001.
[24] Nagata M, Kiyotsukuri T, Minami S, Tsutsumi N, Sakai W. European Polymer Journal 1997;33(10–12):1701–5.
[25] Ellis TS, Karasz FE. Polymer 1984;25:664–9.
[26] Bettinger CJ, Bruggeman JP, Borenstein JT, Langer RS. Biomaterials 2008;29(15):2315–25.
[27] Couchman PR, Karasz FE. Macromolecules 1978;11(1):117–9.
[28] Costa FR, Dutta NK, Choudhury NR, Bhowmick AK. In: Bhowmick AK, editor. Current topics in elastomers research. Boca Raton, FL: CRC Press; 2008.
[29] Liu Q, Tian M, Ding T, Shi R, Feng Y, Zhang L, et al. Journal of Applied Polymer Science 2007;103(3):1412–9.
[30] Liu Q, Tian M, Shi R, Zhang L, Chen D, Tian W. Journal of Applied Polymer Science 2007;104(2):1131–7.
[31] Briggs D, Grant JT. Surface Analysis by Auger and X-ray Photoelectron Spectroscopy. Manchester: IM Publications and Surface Spectra Ltd; 2003.
[32] Chino K, Ashiura M. Macromolecules 2001;34(26):9201–4.
[33] Deslandes N, Bellenger V, Jaffiol F, Verdu J. Journal of Applied Polymer Science 1998;69(13):2663–71.
[34] Tatai L, Moore TG, Adhikari R, Malherbe F, Jayasekara R, Griffiths I, et al. Biomaterials 2007;28(36):5407–17.
[35] Wang Y, Kim YM, Langer R. Journal of Biomedical Materials Research, Part A 2003;66A(1):192–7.